

Collective dipole-dipole interactions in planar nanocavities

Helge Dobbertin,¹ Robert Löw,² and Stefan Scheel^{1,*}

¹*Institut für Physik, Universität Rostock, Albert-Einstein-Straße 23-24, D-18059 Rostock, Germany*

²*Physikalisches Institut and Center for Integrated Quantum Science and Technology, Universität Stuttgart, Pfaffenwaldring 57, 70550 Stuttgart, Germany*

(Dated: July 29, 2020)

The collective response of an atomic ensemble is shaped by its macroscopic environment. We demonstrate this effect in the near-resonant transmission of light through a thermal rubidium vapor confined in a planar nanocavity. Our model reveals density-dependent line shifts and broadenings beyond continuous electrodynamics models that oscillate with cavity width and have been observed in recent experiments. We predict that the amplitudes of these oscillations can be controlled by coatings that modify the cavity's finesse.

When a dense ensemble of quantum emitters is interrogated by near-resonant light, strong dipole-dipole interactions cause a collective response of the system and alter its spectroscopic properties [1–3]. Collective behavior has been studied intensively to build enhanced light-matter interfaces such as a perfect mirror out of a single layer of atoms [4, 5] or to control unwanted effects such as collective line shifts that can bias optical clocks [6–8]. In the past two decades, novel nanophotonic light-matter interfaces were developed [9] that offer new handles to study and tune collective interactions — especially with respect to two parameters: emitter geometry [10, 11] and modification of the local density of states by cavities, waveguides and photonic crystals [12–14].

A prominent example for the geometry-dependence of collective effects is the collective Lamb shift (CLS). Friedberg *et al.* [10] predicted that a continuous slab of atoms of thickness d in free space exhibits a line shift

$$\Delta_{\text{CLS}} = \Delta_{\text{LL}} - \frac{3\Delta_{\text{LL}}}{4} \left(1 - \frac{\sin(2kd)}{2kd} \right). \quad (1)$$

Here, $\Delta_{\text{LL}} = -\frac{N d_{eg}^2}{3\epsilon_0 \hbar (2J_g + 1)}$ is the Lorentz–Lorenz shift that occurs in bulk media, where N is the atomic density, d_{eg} is the transition dipole moment and $(2J_g + 1)$ is the number of (degenerate) ground states. Despite its name, the collective Lamb shift originates from classical single scattering events (see Refs. [15, 16] and below). The CLS has been measured in x-ray scattering from iron layers in a planar cavity [17], whereas cold atomic vapor experiments either found a shift compatible with a CLS prediction [18], or an altogether negligible shift [19–21].

Recently, experiments studied the CLS in wedged nano-cells [11, 16] containing a thermal atomic vapor layer of varying thickness d between two planar walls. This confinement intertwines the sample geometry with the cavity properties and complicates the evaluation of experimental results. Although an earlier study [11] seemed to conform with Eq. (1), an improved analysis revealed that it does not extend to vapors in cavities and

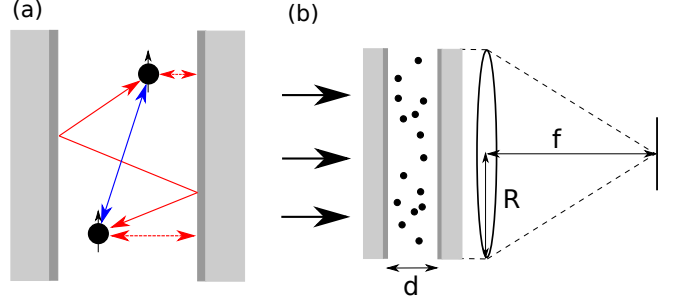


FIG. 1. (a) Free-space (solid blue line) and cavity-mediated (solid red line) atom-atom and atom-wall interactions (dashed lines). (b) Sketch of the setup: Incident light is scattered by atoms in a cavity of width d and focused onto a detector by a lens of radius R .

concluded the agreement to be fortuitous [16]. Instead, the latter study found that the transmission through the vapor-filled nano-cavity can be described by a continuous medium model with an additional broadening and shift that themselves depend on density and cavity width.

In this paper, we present a generalized microscopic interaction model that consistently accounts for the modified non-collisional atom-atom and atom-wall interactions in a planar nanocavity environment. When treating the atomic vapor as a continuous medium, we retrieve the well-known transmission profiles of a Fabry–Perot etalon. When solving our model for discrete ensembles of thermal atoms, the resulting transmission spectra can be fitted to a continuous medium model with an additional collective broadening and shift very similar to the experimental observations in Ref. [16]. We find an oscillatory dependence of the collective broadening and shift on the cavity width. The amplitudes of these oscillatory patterns can be tuned by coatings that increase or decrease the cavity's finesse. This prediction offers a feasible approach for experimental tests. Further, such a test also has implications on collective interactions in other systems of different shape, dimension, or local density of states as the Green's formalism employed here can be adapted to any macroscopic environment.

The scattering of light in atomic samples is most conve-

* stefan.scheel@uni-rostock.de

niently described in a Green's function formalism, where the classical Green's tensor $\mathbf{G}(\mathbf{r}_1, \mathbf{r}_2, \omega)$ is simply the electric field at \mathbf{r}_1 radiated by an electric dipole \mathbf{d} at \mathbf{r}_2 , viz. $\mathbf{E}(\mathbf{r}_1, \omega) = \frac{k^2}{\epsilon_0} \mathbf{G}(\mathbf{r}_1, \mathbf{r}_2, \omega) \mathbf{d}(\mathbf{r}_2, \omega)$. The Green's tensor consists of a free-space and a cavity contribution,

$$\mathbf{G}(\mathbf{r}_1, \mathbf{r}_2, \omega) = \mathbf{G}_{\text{free}}(\mathbf{r}_1, \mathbf{r}_2, \omega) + \mathbf{G}_{\text{cav}}(\mathbf{r}_1, \mathbf{r}_2, \omega). \quad (2)$$

Explicit expressions are provided in the Supplemental Material. If a low-intensity field $\mathbf{E}_{\text{inc}}(\mathbf{r})$ impinges onto an atomic ensemble, the local steady-state response, $\mathbf{d}_i = \mathbf{d}_i^+ + \mathbf{d}_i^-$, follows the classical coupled dipole model (see Supplemental Material)

$$\mathbf{d}_i^\pm = \alpha_i^\pm \mathbf{E}_{\text{inc}}^\pm + \alpha_i^\pm \sum_{j \neq i} \frac{k_0^2}{\epsilon_0} \mathbf{G}(\mathbf{r}_i, \mathbf{r}_j, \omega_0) \mathbf{d}_j^\pm, \quad (3)$$

where ω_0 denotes the single-atom resonance frequency in vacuum and $\mathbf{E}_{\text{inc}}^\pm$ indicates the forward or backward running field components. The dipole moment of atom i is created by the sum of the incident field in an empty cavity, and the field scattered from all other dipoles either directly or via the cavity (see Fig. 1a). Without loss of generality, we take a plane wave polarized along x as input field.

For near-resonant light, the atomic polarizability is well described as a system with two energy levels g, e with degenerate substates μ, ν

$$\alpha_i^\pm = -\frac{1}{\hbar} \sum_{\mu, \nu} \frac{f_{i\mu}^g \mathbf{d}_{\mu\nu}^{ge} \otimes \mathbf{d}_{\nu\mu}^{eg}}{\left[\delta - \Delta_{ge}^\pm(\mathbf{r}_i) + \frac{i}{2} \Gamma_\nu^e(\mathbf{r}_i) \right]}, \quad (4)$$

with ground-state population number $f_{i\mu}^g$, detuning $\delta = \omega - \omega_0$, total line shift $\Delta_{ge}^\pm(\mathbf{r}) = \pm\omega_D + \omega_{\text{CP}\mu\nu}^{ge}(\mathbf{r})$ including the Doppler shift $\omega_D = kv$, and the Purcell-enhanced emission rate $\Gamma_\nu^e(\mathbf{r})$ that depends on the dipole's position and orientation. The modified emission rate is accompanied by a line shift $\omega_{\text{CP}\mu\nu}^{ge}(\mathbf{r})$ deriving from the Casimir-Polder interaction between atoms and cavity walls [22, 23]. We only include the fine structure of the atoms. However, Eq. (4) can be straightforwardly extended to include hyperfine states as well [20].

From the dipole moment in Eq. (3), we compute the transmission profile of the sample. Adopting a method established in free space [24], we consider a lens of radius R (see Fig. 1b), operating in the Fraunhofer limit, that focuses the forward scattered light onto a detector. The lens integrates over the complex field patterns cast by dipoles and allows a compact expression for the transmission coefficient

$$\begin{aligned} t &= t_0 + \frac{\sum_j \frac{k^2}{\epsilon_0} \int_{\text{lens}} dA_j G_{\text{cav, out, xx}}(z, \mathbf{r}_j) d_{x,j}}{\int_{\text{lens}} dA E_0 e^{ik_1 z}} \\ &= t_0 + \frac{2ike^{id\Delta k} t_{21}}{4\pi\epsilon_0 R^2} \sum_j \frac{e^{-ikz_j} + r_{21} e^{ikz_j}}{1 - r_{21}^2 e^{2ikd}} \frac{d_{x,j}}{E_0}, \quad (5) \end{aligned}$$

where t_0 is the transmission through an empty cavity, t_{12}, r_{21} are the Fresnel coefficients at the interfaces of an empty cavity, k_1 is the wavenumber in the cavity material, $\Delta k = k - k_1$, E_0 is the incident field amplitude in free space, and $\mathbf{G}_{\text{cav, out}}$ is the Green's tensor of the light propagating out of the cavity (details of the integration can be found in the Supplemental Material).

When treating the atomic vapor as a continuous medium with a spatially homogeneous polarizability, our model results in the familiar transmission coefficient of a Fabry-Perot etalon. In a high-density vapor, strong line shifts and broadenings exceed the single-body Casimir-Polder and Purcell effects that do not scale with density. In this regime, it is justified to neglect the spatial dependence of the polarizability in Eq. (4). Then, the coupled dipole model (3) results in a field governed by new Fresnel coefficients $\tilde{t}_{12}, \tilde{r}_{21}$ between cavity walls and a gas with refractive index $n_G = \sqrt{1 + N\alpha_{xx}/\epsilon_0}$. Inserting this field into Eq. (5) yields the well-known transmission coefficient of a Fabry-Perot etalon (see Supplemental Material)

$$t = \frac{\tilde{t}_{12} \tilde{r}_{21} e^{id(kn_G - k_1)}}{1 - \tilde{r}_{21}^2 e^{2in_G kd}}. \quad (6)$$

The collective Lamb shift in Eq. (1) derives from the classical Fabry-Perot etalon, Eq. (6), as the limit of a low-density vapor surrounded by free space walls [15, 16]. In this limit Eq. (3) can be solved by the single scattering (first Born) approximation resulting in a Lorentzian transmission profile that features the shift Δ_{CLS} (see also Refs. [15, 16] and Supplemental Material). Deviations from the low-density limit already occur for densities as low as $N = 0.01k^3$ [15]. Therefore, Eq. (1) cannot be used to study the properties of atomic vapors in the intermediate ($N \sim 1k^3$) or dense ($N \gg 1k^3$) regimes, even in free space. On the other hand, the Fabry-Perot relation (6) applies in the dense regime but does not account for the discontinuous distribution of atoms and their mutual correlations [15].

For a full description, we conducted numerical simulations with discrete particles. In each simulation run, we assigned random positions, ground-state populations and Doppler shifts sampled from the Maxwell-Boltzmann distribution to the otherwise static atoms. Then, we found the self-consistent solution to the scattering model (3) for different detunings δ and computed the transmission spectra according to Eq. (5). Finally, we computed the mean over many random atomic realizations until the transmission profile converged. The transmission profiles can be very well fitted to continuum versions of Eqs. (3) and (5) that allow for an additional broadening Γ_p and a line shift Δ_p that are added to the atomic polarizability (4). The fit function also includes non-collisional atom-wall interactions and is detailed in the Supplemental Material. Analogously to the treatment in Ref. [16], the fitting parameters describe all effects that reach beyond the continuous medium model. Repeating the simulations for different densities, we found that Δ_p, Γ_p scale

linearly with density. Their slopes $\partial_N \Delta_p$, $\partial_N \Gamma_p$ describe the non-trivial collective effects in the system.

In the simulations, the slab of atoms was truncated to a cylinder of radius R , with $R = \sqrt{256\pi}/k$ already yielding reasonably well converged fit parameters. We conducted the simulations for the D2 line of ^{85}Rb at room temperature with a Doppler width of $\Delta\omega_{\text{FWHM}} \approx 85\Gamma_0$. Although the polarizability (4) explicitly involves only two energy levels, the Casimir–Polder shift $\omega_{\text{CP}\mu\nu}^{ge}(\mathbf{r}) = \Delta\omega_{5P_{3/2},\nu}(\mathbf{r}) - \Delta\omega_{5S_{1/2},\mu}(\mathbf{r})$ is computed using the full atomic multi-level structure. The Casimir–Polder shift scales asymptotically as $1/R^3$ close to the cavity walls, shifting nearby atoms far away from resonance. This results in an inert layer of gas close to the cavity walls which gradually changes into a normally responding vapor. Under our conditions this normal state is reached about 30 nm away from the surface where the Casimir–Polder shift is comparable to the natural linewidth. This spatially inhomogeneous response alters the transmission profile through the cavity and is included in our fitting function. We performed simulations in a sapphire cavity with and without non-collisional atom-wall interactions and found that the atom-atom interaction parameters $\partial_N \Delta_p$, $\partial_N \Gamma_p$ remain unchanged within the statistical uncertainty. Hence, non-collisional atom-wall interactions do not introduce effects beyond mean-field theory.

As a result, we can introduce dimensionless units based on the two-level structure of the atoms that describe the generic behavior of any alkali vapor by rescaling the cavity size d to the vacuum transition wavelength λ , and the frequency shifts and broadenings to the Lorentz–Lorentz shift Δ_{LL} . Using these dimensionless units, we show in Fig. 2 the results of the ^{85}Rb simulation, together with a recent experiment [16] on ^{39}K vapor where, in both cases, the gas is confined in a sapphire cavity. The error bars of the simulation show the random error of the fits and originate from finite statistics. Whereas the experiment reaches up to atomic densities as high as $100k^3$, our simulations were limited to densities around $1k^3$. This was due to the large numerical effort in solving the system of linear equations (3) that scales as n^3 with the number of atoms n . Further, in the experiment the cell temperature is varied to change the density, and reaches higher values ($T = 600\text{ K}$) using lighter ^{39}K atoms at the same time.

Despite these differences, simulation and experimental results share key features. The experimentally observed collective shift could be represented by cosine function with a period of $(0.5 \pm 0.02)\lambda$ for a cavity size between 0.1λ to 0.75λ [16]. This period approximately matches the series of dips and peaks in the simulation located at 0.52λ , 0.80λ and 1.06λ although the shift does not follow simple analytic function like cosine in regions larger than 0.75λ . The first dip is displaced between simulation and experiment by about 0.1λ but features the same minimal value of $\partial_N \Delta_p = (-1.0 \pm 0.1)\partial_N \Delta_{\text{LL}}$ (experiment) or $\partial_N \Delta_p = (-1.1 \pm 0.1)\partial_N \Delta_{\text{LL}}$ (simulation). The simulated broadening oscillates around the experimental values with quantitative matches in the region between 0.1λ

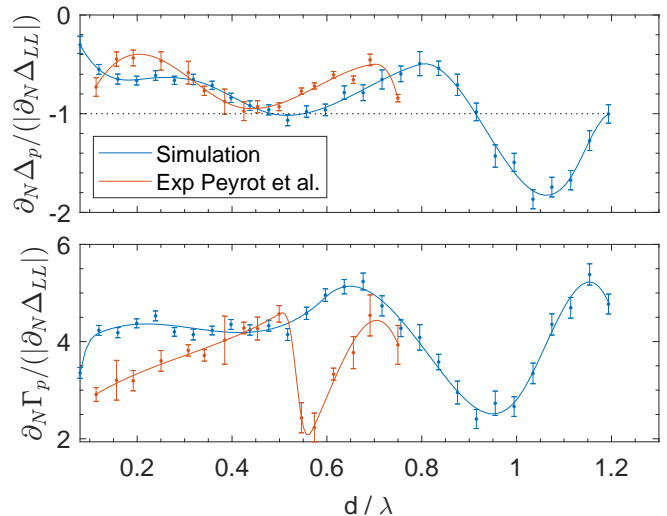


FIG. 2. Slope of collective shift (top) and broadening (bottom) over width d of a vapor-filled sapphire cavity in simulation (^{85}Rb , room temperature, density $\simeq 1k^3$) and experiment [16] (^{39}K , temperature varied up to 600 K, density up to $100k^3$). In textbook electrodynamics, a constant Lorentz-Lorentz shift (dotted line) and no additional broadening is expected. Simulation error bars correspond to 1σ , solid lines are spline interpolations.

and 0.5λ cavity width. As a major difference, the experiment shows a pronounced dip in the broadening around 0.55λ which is not present in the simulation. In sample computations, we found no significant changes to our simulation results when further increasing the temperature. Therefore, the deviations should be considered in the context of four effects that are not covered by the theoretical model.

First, atom-wall collisions change the velocity distribution of the atoms away from a Maxwell–Boltzmann shape as investigated in recent experiments [25]. Once known, the real velocity distribution should be incorporated in the model. Second, the model neglects atom-atom collisions. One could discriminate this effect from the collective broadening by investigating different atomic lines. Whereas the collisional broadening differs by a factor of $\sqrt{2}$ for the D1 and D2 lines [26, 27], the Lorentz–Lorentz shift, and hence the collective broadening, differs by a factor of 2. Third, a moving atom can absorb a photon in one place and radiate at another leading to a non-local susceptibility. This introduces a narrowing of the atomic line at low and intermediate densities [28] including the regime of the simulation $N = (0.1 - 1)k^3$. In the dense regime, where the collective effects are probed, the homogeneous broadening is larger than the Doppler width, $\left|\frac{kv}{kd\Gamma}\right| \ll 1$, and the atomic response becomes local [28]. Therefore, it is consistent to compare the results in Ref. [16] to a simulation that does not account for non-locality. Nonetheless, a full description of experiments conducted at $N \approx 1k^3$ needs to take into account both collective broadening and shift as well as the nonlocal-

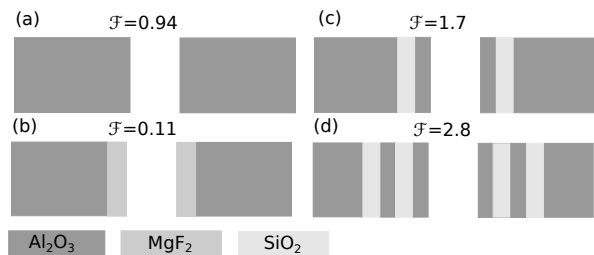


FIG. 3. Cavity designs of finesse \mathcal{F} with (a) no, (b) anti-reflection, or (c),(d) Bragg mirror coating with $\lambda/(4n)$ layers.

ity and should be addressed in a future work. Fourth, we do not account for the finite spectrum of the scattered light, and only incorporate the Doppler shift to 'zeroth' order [15] in the polarizability. However, modeling moving atoms emitting a finite spectrum of light greatly increases the numerical complexity, and no successful implementation of such an approach is known to us.

We attribute the deviations between simulation and experiment mainly to collisions. Considering the importance of collisions to thermal vapors, it is remarkable that the simulation does not only qualitatively retrieve the observed oscillatory pattern of the collective shift but also quantitatively matches its amplitude. We conclude that modified dipole-dipole interactions play the key role in the behavior of the collective shift and broadening and propose an experimental design to test this assertion. It consists of coated cavities that are equipped with distributed Bragg reflectors (DBR) made out of $\lambda/4$ stacks (see Fig. 3c,d). We used a combination of silica ($n = 1.45$) and sapphire ($n = 1.77$) which provides adequate reflectance. With increasing cavity finesse we find a prominent enhancement of the amplitudes of the oscillatory features in the collective shift and broadening as shown in Fig. 4. The oscillatory dependence originates from the constructive or destructive interference of photons that mediate correlated atom-atom interactions. Suppression and enhancement of shift and broadening are therefore increased with higher finesse that sharpens the underlying interference effects. As all cavity designs feature the same sapphire surface, the collisional atom-wall interactions and the resulting changes to the velocity distribution should be the same. Therefore, if future experiments investigate systematic changes in shift and broadening for different cavity designs, the results can be compared against our prediction even without knowledge about the atom-wall collisions.

Complementary to cavities with large finesse, we considered a cavity with an anti-reflection (AR) coating (see Fig. 3b). We chose a $\lambda/4$ magnesium fluoride ($n = 1.38$) layer, which provides decent reflection suppression ($R \approx 0.1\%$). In practice, one would add a thin sapphire layer (~ 10 nm) on top of the AR coating to protect it against the chemically aggressive alkali vapor [29]. The collective shift and broadening in the AR-coated cavity shown

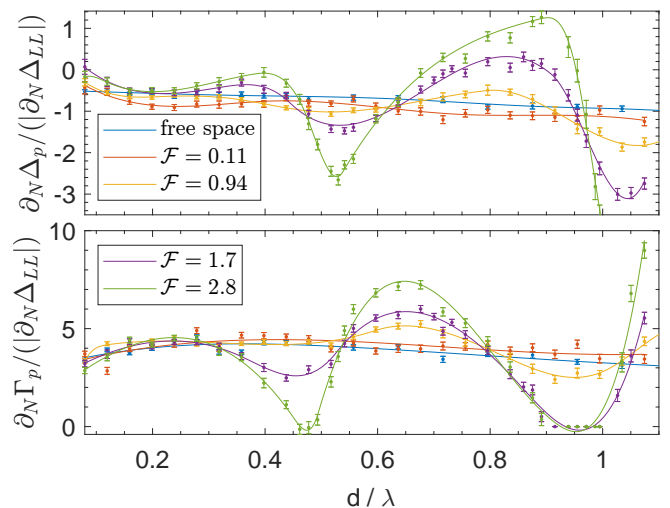


FIG. 4. Slope of collective shift (top) and broadening (bottom) over width d of atomic layer in free space and in the coated cavities depicted in Fig. 3. Error bars correspond to 1σ , solid lines are spline interpolations.

in Fig. 4 no longer feature pronounced oscillations which can be attributed to the fact that the AR coating suppresses photonic interference in the cavity. However, the results for the AR-coated cavity still deviate from results obtained in free space. Although the AR coating suppresses reflection at normal incidence, the light fields exchanged between atoms also involve finite oblique reflection that modify atom-atom interactions.

The presented model is not exclusive to thermal vapor but also applies to ultracold atoms. However, one finds that at low temperatures ($T < 1$ K) the resulting transmission profiles can no longer be described by continuum models, even when introducing more fit parameters such as an effective density. As a result, one cannot easily predict or discriminate to which amount a line shift is caused by mean-field effects as contained in Eq. (6), or by additional collective effects. This may be one reason for the seemingly conflicting outcomes of cold vapor experiments mentioned above.

In conclusion, we constructed a microscopic model that accounts for the effects of a macroscopic cavity environment on the dipole-dipole interaction between atoms. We showed that these modified interactions can explain the oscillatory dependence of the collective shift of thermal atoms on the cavity width observed in Ref. [16]. Furthermore, we predicted that the amplitudes of these oscillations can be tuned in coated cavities which can be tested in future experiments. The existing literature has explored the atom-atom interactions in one- and two-dimensional photonic crystals [12–14], and is now complemented by our three-dimensional description. Our model can be used to evaluate the role of dipole-dipole interactions, Casimir–Polder and Purcell effects in many macroscopic environments that have been interfaced with atoms such as microresonators [30], nanofibers

[31], hollow-core fibers [32], superconducting chips [33], and atomic cladding waveguides [29, 34]. The necessary changes have to be incorporated in the respective Green's tensor. In a next step, our model should be extended to account for nonlocal susceptibilities and saturation effects that are more likely to occur in cavity environments. The difficulties to reproduce the bulk Lorentz–Lorenz shift in thermal vapors in free space raised questions as to whether the microscopic modeling of atom–atom interactions can be considered complete [15]. We

hope that future tests to our model can help address this fundamental question.

ACKNOWLEDGMENTS

We thank Charles Adams and Robin Kaiser for fruitful discussions and Tom Peyrot for sharing his data and insights on the topic with us.

-
- [1] Robert H Dicke, “Coherence in spontaneous radiation processes,” *Phys. Rev.* **93**, 99 (1954).
- [2] Marlan O Scully, “Collective lamb shift in single photon dicke superradiance,” *Phys. Rev. Lett.* **102**, 143601 (2009).
- [3] William Guerin, Michelle O Araújo, and Robin Kaiser, “Subradiance in a large cloud of cold atoms,” *Phys. Rev. Lett.* **116**, 083601 (2016).
- [4] Robert J Bettles, Simon A Gardiner, and Charles S Adams, “Enhanced optical cross section via collective coupling of atomic dipoles in a 2d array,” *Phys. Rev. Lett.* **116**, 103602 (2016).
- [5] Ephraim Shahmoon, Dominik S Wild, Mikhail D Lukin, and Susanne F Yelin, “Cooperative resonances in light scattering from two-dimensional atomic arrays,” *Phys. Rev. Lett.* **118**, 113601 (2017).
- [6] D E Chang, Jun Ye, and M D Lukin, “Controlling dipole-dipole frequency shifts in a lattice-based optical atomic clock,” *Phys. Rev. A* **69**, 023810 (2004).
- [7] Sarah L Bromley, Bihui Zhu, Michael Bishof, Xibo Zhang, Tobias Bothwell, Johannes Schachenmayer, Travis L Nicholson, Robin Kaiser, Susanne F Yelin, Mikhail D Lukin, A M Rey, and Jun Ye, “Collective atomic scattering and motional effects in a dense coherent medium,” *Nat. Commun.* **7**, 11039 (2016).
- [8] Sara L Campbell, R B Hutson, G E Marti, A Goban, N Darkwah Oppong, R L McNally, L Sonderhouse, J M Robinson, W Zhang, B J Bloom, and Jun Ye, “A fermi-degenerate three-dimensional optical lattice clock,” *Science* **358**, 90–94 (2017).
- [9] D E Chang, J S Douglas, Alejandro González-Tudela, C-L Hung, and H J Kimble, “Colloquium: Quantum matter built from nanoscopic lattices of atoms and photons,” *Rev. Mod. Phys.* **90**, 031002 (2018).
- [10] Richard Friedberg, Sven Richard Hartmann, and Jamal T Manassah, “Frequency shifts in emission and absorption by resonant systems of two-level atoms,” *Phys. Rep.* **7**, 101–179 (1973).
- [11] James Keaveney, Armen Sargsyan, Ulrich Krohn, Ifan G Hughes, David Sarkisyan, and Charles S Adams, “Cooperative lamb shift in an atomic vapor layer of nanometer thickness,” *Phys. Rev. Lett.* **108**, 173601 (2012).
- [12] Janne Ruostekoski and Juha Javanainen, “Emergence of correlated optics in one-dimensional waveguides for classical and quantum atomic gases,” *Phys. Rev. Lett.* **117**, 143602 (2016).
- [13] A Goban, C-L Hung, J D Hood, S-P Yu, J A Muniz, O Painter, and H J Kimble, “Superradiance for atoms trapped along a photonic crystal waveguide,” *Phys. Rev. Lett.* **115**, 063601 (2015).
- [14] Alejandro González-Tudela, C-L Hung, Darrick E Chang, J Ignacio Cirac, and H J Kimble, “Subwavelength vacuum lattices and atom–atom interactions in two-dimensional photonic crystals,” *Nat. Photonics* **9**, 320 (2015).
- [15] Juha Javanainen, Janne Ruostekoski, Yi Li, and Sung-Mi Yoo, “Exact electrodynamics versus standard optics for a slab of cold dense gas,” *Phys. Rev. A* **96**, 033835 (2017).
- [16] Tom Peyrot, Y R P Sortais, A Browaeys, Armen Sargsyan, David Sarkisyan, J Keaveney, I G Hughes, and Charles S Adams, “Collective lamb shift of a nanoscale atomic vapor layer within a sapphire cavity,” *Phys. Rev. Lett.* **120**, 243401 (2018).
- [17] Ralf Röhlsberger, Kai Schlage, Balaram Sahoo, Sebastien Couet, and Rudolf Ruffer, “Collective lamb shift in single-photon superradiance,” *Science* **328**, 1248–1251 (2010).
- [18] S J Roof, K J Kemp, M D Havey, and I M Sokolov, “Observation of single-photon superradiance and the cooperative lamb shift in an extended sample of cold atoms,” *Phys. Rev. Lett.* **117**, 073003 (2016).
- [19] J Pellegrino, R Bourgain, Stephan Jennewein, Yvan R P Sortais, Antoine Browaeys, S D Jenkins, and J Ruostekoski, “Observation of suppression of light scattering induced by dipole-dipole interactions in a cold-atom ensemble,” *Phys. Rev. Lett.* **113**, 133602 (2014).
- [20] S D Jenkins, J Ruostekoski, J Javanainen, S Jennewein, R Bourgain, J Pellegrino, Yvan R P Sortais, and Antoine Browaeys, “Collective resonance fluorescence in small and dense atom clouds: Comparison between theory and experiment,” *Phys. Rev. A* **94**, 023842 (2016).
- [21] Laura Corman, Jean-Loup Ville, Raphaël Saint-Jalm, Monika Aidelsburger, Tom Bienaimé, Sylvain Nascimbène, Jean Dalibard, and Jérôme Beugnon, “Transmission of near-resonant light through a dense slab of cold atoms,” *Phys. Rev. A* **96**, 053629 (2017).
- [22] Stefan Yoshi Buhmann, *Dispersion forces I: Macroscopic quantum electrodynamics and ground-state Casimir, Casimir–Polder and van der Waals Forces*, Vol. 247 (Springer, 2013).
- [23] Stefan Yoshi Buhmann, *Dispersion Forces II: Many-Body Effects, Excited Atoms, Finite Temperature and Quantum Friction*, Vol. 248 (Springer, 2013).
- [24] Lauriane Chomaz, Laura Corman, Tarik Yefsah, Rémi Desbuquois, and Jean Dalibard, “Absorption imaging of a quasi-two-dimensional gas: a multiple scattering analysis,” *New J. Phys.* **14**, 055001 (2012).

- [25] Petko Todorov and Daniel Bloch, “Testing the limits of the Maxwell distribution of velocities for atoms flying nearly parallel to the walls of a thin cell,” *J. Chem. Phys.* **147**, 194202 (2017).
- [26] E L Lewis, “Collisional relaxation of atomic excited states, line broadening and interatomic interactions,” *Phys. Rep.* **58**, 1–71 (1980).
- [27] Lee Weller, Robert J Bettles, Paul Siddons, Charles S Adams, and Ifan G Hughes, “Absolute absorption on the rubidium d1 line including resonant dipole–dipole interactions,” *J. Phys. B* **44**, 195006 (2011).
- [28] T Peyrot, Y R P Sortais, J-J Greffet, A Browaeys, A Sargsyan, J Keaveney, I G Hughes, and C S Adams, “Optical transmission of an atomic vapor in the mesoscopic regime,” *Phys. Rev. Lett.* **122**, 113401 (2019).
- [29] Ralf Ritter, Nico Gruhler, Helge Dobbertin, Harald Kübler, Stefan Scheel, Wolfram Pernice, Tilman Pfau, and Robert Löw, “Coupling thermal atomic vapor to slot waveguides,” *Phys. Rev. X* **8**, 021032 (2018).
- [30] D W Vernooy, A Furusawa, N Ph Georgiades, V S Ilchenko, and H J Kimble, “Cavity qed with high-q whispering gallery modes,” *Phys. Rev. A* **57**, R2293 (1998).
- [31] E Vetsch, D Reitz, G Sagué, R Schmidt, S T Dawkins, and A Rauschenbeutel, “Optical interface created by laser-cooled atoms trapped in the evanescent field surrounding an optical nanofiber,” *Phys. Rev. Lett.* **104**, 203603 (2010).
- [32] Saikat Ghosh, Amar R Bhagwat, C Kyle Renshaw, Shireen Goh, Alexander L Gaeta, and Brian J Kirby, “Low-light-level optical interactions with rubidium vapor in a photonic band-gap fiber,” *Phys. Rev. Lett.* **97**, 023603 (2006).
- [33] H Hattermann, D Bothner, L Y Ley, B Ferdinand, D Wiedmaier, L Sárkány, Reinhold Kleiner, Dieter Koelle, and J Fortágh, “Coupling ultracold atoms to a superconducting coplanar waveguide resonator,” *Nat. Commun.* **8**, 2254 (2017).
- [34] Liron Stern, Boris Desiatov, Ilya Goykhman, and Uriel Levy, “Nanoscale light–matter interactions in atomic cladding waveguides,” *Nat. Commun.* **4**, 1548 (2013).
- [35] Ho Trung Dung, Ludwig Knöll, and Dirk-Gunnar Welsch, “Resonant dipole-dipole interaction in the presence of dispersing and absorbing surroundings,” *Physical Review A* **66**, 063810 (2002).
- [36] Stefan Yoshi Buhmann, Ludwig Knöll, Dirk-Gunnar Welsch, and Ho Trung Dung, “Casimir-polder forces: A nonperturbative approach,” *Physical Review A* **70**, 052117 (2004).
- [37] Mark D Lee, Stewart D Jenkins, and Janne Ruostekoski, “Stochastic methods for light propagation and recurrent scattering in saturated and nonsaturated atomic ensembles,” *Physical Review A* **93**, 063803 (2016).
- [38] Michael Paulus, Phillipe Gay-Balmaz, and Olivier J F Martin, “Accurate and efficient computation of the greens tensor for stratified media,” *Phys. Rev. E* **62**, 5797 (2000).

Supplemental Material: Collective dipole-dipole interactions in planar nanocavities

Helge Dobbertin,¹ Robert Löw,² and Stefan Scheel^{1,*}

¹*Institut für Physik, Universität Rostock, Albert-Einstein-Straße 23-24, D-18059 Rostock, Germany*

²*5. Physikalisches Institut and Center for Integrated Quantum Science and Technology, Universität Stuttgart, Pfaffenwaldring 57, 70550 Stuttgart, Germany*

(Dated: July 29, 2020)

I. DERIVATION OF THE COUPLED DIPOLE MODEL

In this section, we derive the coupled dipole model from quantum theory. We start with the atom-field coupling Hamiltonian in dipole approximation [1, 2]

$$\hat{H} = \int d^3\mathbf{r} \int_0^\infty d\omega \hat{\mathbf{f}}^\dagger(\mathbf{r}, \omega) \cdot \hat{\mathbf{f}}(\mathbf{r}, \omega) \hbar\omega + \sum_A \sum_n E_{A,n} \hat{\sigma}_{A,nn} - \sum_A \int_0^\infty d\omega [\hat{\mathbf{d}}_A \cdot \hat{\mathbf{E}}(\mathbf{r}_A, \omega) + \hat{\mathbf{E}}^\dagger(\mathbf{r}_A, \omega) \cdot \hat{\mathbf{d}}_A], \quad (\text{S1})$$

where $\hat{\mathbf{d}}_A = \sum_{m,n} \mathbf{d}_{A,mn} \hat{\sigma}_{A,mn}$ and $\hat{\sigma}_{A,mn} = |m_A\rangle \langle n_A|$ are the atomic transition operators. The equation of motion for the atomic operators becomes

$$\begin{aligned} \dot{\hat{\sigma}}_{A,mn} = \frac{1}{i\hbar} [\hat{\sigma}_{A,mn}, \hat{H}] = & -i\omega_{A,nm} \hat{\sigma}_{A,mn} + \frac{i}{\hbar} \int_0^\infty d\omega \left[\sum_k (\hat{\sigma}_{A,mk} \mathbf{d}_{A,nk} - \hat{\sigma}_{A,kn} \mathbf{d}_{A,km}) \cdot \hat{\mathbf{E}}(\mathbf{r}_A, \omega) \right. \\ & \left. + \hat{\mathbf{E}}^\dagger(\mathbf{r}_A, \omega) \cdot \sum_k (\hat{\sigma}_{A,mk} \mathbf{d}_{A,nk} - \hat{\sigma}_{A,kn} \mathbf{d}_{A,km}) \right], \end{aligned} \quad (\text{S2})$$

where $\omega_{A,nm} = [E_{A,n} - E_{A,m}]/\hbar$. We expand the electric field operator in terms of the Green's function $\mathbf{G}(\mathbf{r}, \mathbf{r}', \omega)$ and a set of bosonic vector fields $\hat{\mathbf{f}}(\mathbf{r}, \omega)$ describing collective excitations of the electromagnetic field and the linearly absorbing matter [1, 2]

$$\hat{\mathbf{E}}(\mathbf{r}, \omega) = i \sqrt{\frac{\hbar}{\pi\epsilon_0}} \frac{\omega^2}{c^2} \int d^3\mathbf{r}' \sqrt{\text{Im} \epsilon(\mathbf{r}', \omega)} \mathbf{G}(\mathbf{r}, \mathbf{r}', \omega) \hat{\mathbf{f}}(\mathbf{r}', \omega), \quad (\text{S3})$$

and solve its equation of motion in Markov approximation leading to [1, 2]

$$\hat{\mathbf{E}}(\mathbf{r}, \omega, t) = e^{-i\omega t} \hat{\mathbf{E}}(\mathbf{r}, \omega, 0) + i\mu_0 \sum_A \sum_{m,n} \left(\delta(\omega - \tilde{\omega}_{A,nm}) - \frac{i}{\pi} \frac{\mathcal{P}}{\omega - \tilde{\omega}_{A,nm}} \right) \omega^2 \text{Im} \mathbf{G}(\mathbf{r}, \mathbf{r}_A(t), \omega) \mathbf{d}_{A,mn} \hat{\sigma}_{A,mn}(t). \quad (\text{S4})$$

Here, we introduced the effective frequencies $\tilde{\omega}_{A,nm}$ that govern the time evolution of the atomic operators due to the atom-field interactions, and that can be determined self-consistently later. We insert the field back into Eq. (S2) and explicitly denote the coherence between degenerate substates ν, μ of the energy levels n, m by $\hat{\sigma}_{A,\nu\mu}^{nm}$. Its expectation value becomes

$$\begin{aligned} \langle \dot{\hat{\sigma}}_{A,\mu\nu}^{ge} \rangle = & i\omega_{A,ge} \langle \hat{\sigma}_{A,\mu\nu}^{ge} \rangle + \frac{i}{\hbar} \sum_k \left\{ \langle \hat{\sigma}_{A,\mu\kappa}^{gk} \rangle \mathbf{d}_{A,\nu\kappa}^{ek} - \langle \hat{\sigma}_{A,\kappa\nu}^{ke} \rangle \mathbf{d}_{A,\kappa\mu}^{kg} \right\} \cdot \mathbf{E}_{\text{inc}}(\mathbf{r}_A, t) \\ & + \sum_B \sum_{kpq} \left\{ \left(\langle \hat{\sigma}_{A,\mu\kappa}^{gk} \hat{\sigma}_{B,\delta\epsilon}^{pq} \rangle \mathbf{d}_{A,\nu\kappa}^{ek} - \langle \hat{\sigma}_{A,\kappa\nu}^{ke} \hat{\sigma}_{B,\delta\epsilon}^{pq} \rangle \mathbf{d}_{A,\kappa\mu}^{kg} \right) \cdot \left(-\frac{1}{2} \mathcal{A}_{B,qp}(\mathbf{r}_A, \mathbf{r}_B) - i\mathcal{B}_{B,qp}(\mathbf{r}_A, \mathbf{r}_B) \right) \mathbf{d}_{B,\delta\epsilon}^{pq} \right. \\ & \left. + \mathbf{d}_{B,\delta\epsilon}^{qp} \cdot \left(\frac{1}{2} \mathcal{A}_{B,qp}(\mathbf{r}_B, \mathbf{r}_A) - i\mathcal{B}_{B,qp}(\mathbf{r}_B, \mathbf{r}_A) \right) \left(\langle \hat{\sigma}_{B,\delta\epsilon}^{qp} \hat{\sigma}_{A,\mu\kappa}^{gk} \rangle \mathbf{d}_{A,\nu\kappa}^{ek} - \langle \hat{\sigma}_{B,\delta\epsilon}^{qp} \hat{\sigma}_{A,\kappa\nu}^{ke} \rangle \mathbf{d}_{A,\kappa\mu}^{kg} \right) \right\}, \end{aligned} \quad (\text{S5})$$

* stefan.scheel@uni-rostock.de

where we introduced the abbreviations

$$\mathcal{A}_{A,nm}(\mathbf{r}, \mathbf{r}') = \frac{2\mu_0}{\hbar} \Theta(\tilde{\omega}_{A,nm}) \tilde{\omega}_{A,nm}^2 \text{Im} \mathbf{G}(\mathbf{r}, \mathbf{r}', \tilde{\omega}_{A,nm}), \quad (\text{S6})$$

$$\begin{aligned} \mathcal{B}_{A,nm}(\mathbf{r}, \mathbf{r}') &= -\frac{\mu_0}{\hbar\pi} \mathcal{P} \int_0^\infty d\omega \frac{\omega^2 \text{Im} \mathbf{G}(\mathbf{r}, \mathbf{r}', \omega)}{\omega - \tilde{\omega}_{A,nm}} \\ &= -\frac{\mu_0}{\hbar} \Theta(\tilde{\omega}_{A,nm}) \tilde{\omega}_{A,nm}^2 \text{Re} \mathbf{G}(\mathbf{r}, \mathbf{r}', \tilde{\omega}_{A,nm}) - \frac{\mu_0}{\hbar\pi} \int_0^\infty d\xi \frac{\tilde{\omega}_{A,nm}}{\tilde{\omega}_{A,nm}^2 + \xi^2} \xi^2 \mathbf{G}(\mathbf{r}, \mathbf{r}', i\xi). \end{aligned} \quad (\text{S7})$$

We define the Casimir–Polder line shift and the corresponding Purcell decay rate as

$$\Delta\omega_{A\nu\delta}^n = \sum_k \mathbf{d}_{A\nu\kappa}^{nk} \cdot \mathcal{B}_{A,nk}(\mathbf{r}, \mathbf{r}) \mathbf{d}_{A\kappa\delta}^{kn}, \quad \Gamma_{A\nu\delta}^n = \sum_k \mathbf{d}_{A\nu\kappa}^{nk} \cdot \mathcal{A}_{A,nk}(\mathbf{r}, \mathbf{r}) \mathbf{d}_{A\kappa\delta}^{kn}. \quad (\text{S8})$$

Assuming that the modification of the resonance frequency due to interactions is small compared to the bare resonance frequency, we can replace $\tilde{\omega}_{A,nm} \mapsto \omega_{A,nm}$ in the definition of $\mathcal{A}_{A,nm}(\mathbf{r}, \mathbf{r}')$ and $\mathcal{B}_{A,nm}(\mathbf{r}, \mathbf{r}')$ and compute the line shifts and decay rates perturbatively.

In order to retrieve the classical coupled dipole model, three classical assumptions are necessary [3]. First, we assume that we start from and remain in an incoherent mixture of ground states $\langle \hat{\sigma}_{A\mu\nu}^{gg} \rangle = \delta_{\mu\nu} f_{A\mu}^g$ with occupation numbers $f_{A\mu}^g$. Second, we assume that the ground-state population of atom A is not correlated to the coherence of atom B , i.e. $\langle \hat{\sigma}_{A\mu\nu}^{gg} \hat{\sigma}_{B\delta\epsilon}^{ge} \rangle = \langle \hat{\sigma}_{A\mu\nu}^{gg} \rangle \langle \hat{\sigma}_{B\delta\epsilon}^{ge} \rangle$ when $A \neq B$. Third, we assume that the atoms are unsaturated, and hence all excited states are not significantly populated. Furthermore, we assume a monochromatic incident field with frequency ω_L , i.e. $\mathbf{E}_{\text{inc}}(\mathbf{r}, t) = \mathbf{E}_{\text{inc}}(\mathbf{r}) e^{-i\omega_L t}$. Then, we transform the equation of motion into the rotating frame of the incident field leading to the slowly varying coherence amplitude $\langle \hat{\sigma}_{A\mu\nu}^{ge} \rangle = e^{i\omega_L t} \langle \hat{\sigma}_{A\mu\nu}^{ge} \rangle$. Assuming that the incident light is near-resonant to the $e \leftrightarrow g$ transition but far detuned from all other atomic transitions, we discard other $\langle \hat{\sigma}_{B\delta\epsilon}^{qp} \rangle$ terms in rotating-wave approximation. The effective equation of motion becomes

$$\begin{aligned} \langle \dot{\hat{\sigma}}_{A\mu\nu}^{ge} \rangle &= i(\omega_L - \omega_{A,eg}) \langle \hat{\sigma}_{A\mu\nu}^{ge} \rangle + \frac{i}{\hbar} f_{A\mu}^g \mathbf{d}_{A\mu\nu}^* \cdot \mathbf{E}_{\text{inc}}(\mathbf{r}_A) \\ &+ i \sum_\delta (-\Delta\omega_{A\nu\delta}^e + \frac{i}{2} \Gamma_{A\nu\delta}^e) \langle \hat{\sigma}_{A\mu\delta}^{ge} \rangle + i \sum_\delta (\Delta\omega_{A\delta\mu}^g + \frac{i}{2} \Gamma_{A\delta\mu}^g) \langle \hat{\sigma}_{A\delta\nu}^{ge} \rangle \\ &+ \frac{i\mu_0}{\hbar} \tilde{\omega}_{A,eg}^2 f_{A\mu}^g \sum_{A \neq B} \sum_{\delta, \epsilon} \mathbf{d}_{A\nu\mu}^{eg} \cdot \mathbf{G}(\mathbf{r}_A, \mathbf{r}_B, \tilde{\omega}_{A,eg}) \mathbf{d}_{B\delta\epsilon}^{ge} \langle \hat{\sigma}_{B\delta\epsilon}^{ge} \rangle. \end{aligned} \quad (\text{S9})$$

Different coherences of a single atom $\langle \hat{\sigma}_{A\mu\nu}^{ge} \rangle$, $\langle \hat{\sigma}_{A\epsilon\delta}^{ge} \rangle$ can mutually couple when an atom emits and reabsorbs a photon that in between has changed its polarization after being reflected from a macroscopic body. In our planar cavity system, the Green's tensor $\mathbf{G}(\mathbf{r}, \mathbf{r}, \omega) = \text{diag}(G^\parallel(\mathbf{r}, \mathbf{r}, \omega), G^\parallel(\mathbf{r}, \mathbf{r}, \omega), G^\perp(\mathbf{r}, \mathbf{r}, \omega))$ is diagonal and the z-axis is chosen perpendicular to the surface. We take the quantization axis of the atoms along the z-direction and encounter no coupling, i.e. $\Delta\omega_{A\nu\delta, z}^k = \Gamma_{A\nu\delta, z}^k = 0, \forall \nu \neq \delta$. When the quantization axis is chosen along the x-direction parallel to the surface, coupling occurs, e.g. $\Delta\omega_{A\nu\delta, x}^e \neq 0$ for $\nu = -3/2, \delta = +1/2$ because $G^\perp(\mathbf{r}, \mathbf{r}, \omega) - G^\parallel(\mathbf{r}, \mathbf{r}, \omega) \neq 0$. Then, a linear equation system has to be solved. Depending on the choice of basis, the individual sublevels may experience different shifts and broadenings. However, the polarizability, which sums over all sublevels, is the same in all bases. Introducing the abbreviation $\Gamma_{A\nu}^e \equiv \Gamma_{A\nu\nu}^e$, the operator equation of motion with a quantization axis in z-direction becomes

$$\begin{aligned} \langle \dot{\hat{\sigma}}_{A\mu\nu}^{ge} \rangle &= i \left(\omega_L - \omega_{A,eg} - \Delta\omega_{A\nu}^e + \Delta\omega_{A\mu}^g + \frac{i}{2} [\Gamma_{A\nu}^e + \Gamma_{A\mu}^g] \right) \langle \hat{\sigma}_{A\mu\nu}^{ge} \rangle + \frac{i}{\hbar} f_{A\mu}^g \mathbf{d}_{A\mu\nu}^* \cdot \mathbf{E}_{\text{inc}}(\mathbf{r}_A) \\ &+ \frac{i\mu_0}{\hbar} \tilde{\omega}_{A,eg}^2 f_{A\mu}^g \sum_{A \neq B} \sum_{\delta, \epsilon} \mathbf{d}_{A\nu\mu}^{eg} \cdot \mathbf{G}(\mathbf{r}_A, \mathbf{r}_B, \tilde{\omega}_{A,eg}) \mathbf{d}_{B\delta\epsilon}^{ge} \langle \hat{\sigma}_{B\delta\epsilon}^{ge} \rangle. \end{aligned} \quad (\text{S10})$$

Casimir–Polder and Purcell effects generally depend on temperature [4]. In our setting the room temperature provides no significant population of the atomic energy levels. Additionally, the separation between atoms and surface never becomes larger than the transition wavelength, and thus remains small compared to the wavelength of thermal photons. Therefore, both the spectroscopic and geometric temperature are low and our zero temperature treatment of dispersion interactions is justified.

The thermal motion of the atoms is accounted for by the hydrodynamic derivative $\frac{d}{dt} \langle \hat{\sigma}_{A\mu\nu}^{ge} \rangle = \frac{\partial}{\partial t} \langle \hat{\sigma}_{A\mu\nu}^{ge} \rangle + \mathbf{v} \cdot \nabla \langle \hat{\sigma}_{A\mu\nu}^{ge} \rangle$. The spatial dependence introduced by the incident field, $\mathbf{E}_{\text{inc}}(\mathbf{r}) = \tilde{\mathbf{E}}_{\text{inc}}^+ e^{ikz} + \tilde{\mathbf{E}}_{\text{inc}}^- e^{-ikz}$, can be accounted for by an ansatz $\langle \hat{\sigma}_{A\mu\nu}^{ge} \rangle = \langle \hat{\sigma}_{A\mu\nu}^{ge+} \rangle e^{ikz} + \langle \hat{\sigma}_{A\mu\nu}^{ge-} \rangle e^{-ikz}$. The original equation of motion is the sum of two sets of equations for $\langle \hat{\sigma}_{A\mu\nu}^{\pm} \rangle$,

$$\begin{aligned} \langle \partial_t \hat{\sigma}_{A\mu\nu}^{\pm} \rangle + \mathbf{v} \cdot \nabla \langle \hat{\sigma}_{A\mu\nu}^{\pm} \rangle = & i \left(\omega_L - \omega_{A,eg} \mp kv_z - \Delta\omega_{A\nu}^e + \Delta\omega_{A\mu}^g + \frac{i}{2} \left[\Gamma_{A\nu}^e + \Gamma_{A\mu}^g \right] \right) \langle \hat{\sigma}_{A\mu\nu}^{\pm} \rangle + \frac{i}{\hbar} f_{A\mu}^g \mathbf{d}_{A\mu\nu}^{ge*} \cdot \tilde{\mathbf{E}}_{\text{inc}}^{\pm} \\ & + \frac{i\mu_0}{\hbar} \tilde{\omega}_{A,eg}^2 f_{A\mu}^g \sum_{A \neq B} \sum_{\delta, \epsilon} \mathbf{d}_{A\nu\mu}^{eg} \cdot \mathbf{G}(\mathbf{r}_A, \mathbf{r}_B, \tilde{\omega}_{A,eg}) \mathbf{d}_{B\delta\epsilon}^{ge} \langle \hat{\sigma}_{B\delta\epsilon}^{\pm} \rangle e^{\pm ik(z_B - z_A)}. \end{aligned} \quad (\text{S11})$$

We assume the local limit, i.e. $\left| \frac{\mathbf{v}}{d\Gamma_{A\nu}^e} \right| \ll 1$, where d is the thickness of the atomic vapor layer, and neglect the term $\mathbf{v} \cdot \nabla \langle \hat{\sigma}_{A\mu\nu}^{\pm} \rangle$ which describes that atoms re-emit light at a position different from their original spot of excitation [5]. In the steady state, $\langle \partial_t \hat{\sigma}_{A\mu\nu}^{ge} \rangle = 0$, one obtains a linear set of equations for the $\langle \hat{\sigma}_{A\mu\nu}^{\pm} \rangle$. Identifying the classical dipole moment with the expectation value $\langle \tilde{\mathbf{d}}_{A,ge} \rangle = \sum_{\mu, \nu} \langle \hat{\sigma}_{A\mu\nu}^{ge} \rangle \mathbf{d}_{A\mu\nu}^{ge}$ and introducing $\mathbf{E}_{\text{inc}}^{\pm} = \tilde{\mathbf{E}}_{\text{inc}}^{\pm} e^{\pm ikz}$, we arrive at Eq. (3) of the main text.

II. EXPLICIT FORM OF THE GREEN'S TENSOR FOR A PLANAR CAVITY

The Green's tensor is the unique solution of the Helmholtz equation

$$\left[\nabla \times \nabla \times - k^2 \varepsilon(\mathbf{r}_1, \omega) \right] \mathbf{G}(\mathbf{r}_1, \mathbf{r}_2, \omega) = \delta(\mathbf{r}_1 - \mathbf{r}_2), \quad (\text{S12})$$

with the Sommerfeld radiation boundary condition $\mathbf{G}(\mathbf{r}_1, \mathbf{r}_2, \omega) \rightarrow \mathbf{0}$ when $|\mathbf{r}| \rightarrow \infty$ where $\mathbf{r} = \mathbf{r}_1 - \mathbf{r}_2$. The free-space (bulk) part of the Green's tensor can be expressed as [6]

$$\mathbf{G}_{\text{free}}(\mathbf{r}_1, \mathbf{r}_2, \omega) = -\frac{\delta(\mathbf{r})}{3k^2} + \frac{e^{ikr}}{4\pi k^2 r^3} \left[(k^2 r^2 + ikr - 1) \mathbf{I} + (3 - 3ikr - k^2 r^2) \mathbf{e}_r \otimes \mathbf{e}_r \right]. \quad (\text{S13})$$

Next, we derive the cavity (scattering) contribution $\mathbf{G}_{\text{cav}}(\mathbf{r}_1, \mathbf{r}_2, \omega)$ in Eq. (2). Due to cylindrical symmetry, we can utilize a coordinate system in which the source is located at $\mathbf{r}_2 = (0, 0, z_2)$, the receiver at $\mathbf{r}_1 = (x, 0, z_1)$, with the z -axis perpendicular to the surfaces. Any other pair of points can be transformed to this set of coordinates. By defining the distance $x = \sqrt{(x_1 - x_2)^2 + (y_1 - y_2)^2}$ and the angle $\cos \phi = (x_1 - x_2)/x$ to the x -axis, we can write the Green's tensor as

$$\mathbf{G}_{\text{cav}}(\mathbf{r}_1, \mathbf{r}_2, \omega) = \mathbf{G}_{\text{cav}}(x, \phi, z_1, z_2, \omega) = \mathbf{R}^T(\phi) \mathbf{G}_{\text{cav}}(x, z_1, z_2, \omega) \mathbf{R}(\phi), \quad (\text{S14})$$

$$\mathbf{R}(\phi) = \begin{pmatrix} \cos \phi & -\sin \phi & 0 \\ \sin \phi & \cos \phi & 0 \\ 0 & 0 & 1 \end{pmatrix}. \quad (\text{S15})$$

Next, $\mathbf{G}_{\text{cav}}(x, z_1, z_2, \omega)$ is constructed in the basis of s - and p -polarised plane waves [6]. We decompose the wavevector in layer j ($j = 1$ outside and $j = 2$ inside the cavity, see Fig. 1) into components parallel and orthogonal to the surface, $\mathbf{k}_j = \mathbf{k}_j^{\parallel} + \mathbf{k}_j^{\perp}$. Using cylindrical coordinates $\mathbf{k}_j^{\parallel} = k_j^{\parallel} (\cos \phi_k, \sin \phi_k, 0)^T$, we write the basis as

$$\mathbf{e}_{s\pm}^j = \mathbf{e}_{k_j^{\parallel}} \times \mathbf{e}_z = (\sin \phi_k, -\cos \phi_k, 0)^T, \quad (\text{S16})$$

$$\mathbf{e}_{p\pm}^j = \frac{1}{k_j} (k_j^{\parallel} \mathbf{e}_z \mp k_j^{\perp} \mathbf{e}_{k_j^{\parallel}}) = \frac{1}{k_j} (\mp k_j^{\perp} \cos \phi_k, \mp k_j^{\perp} \sin \phi_k, k_j^{\parallel})^T. \quad (\text{S17})$$

Considering the different pathways connecting source and receiver sketched in Fig. 1, we can write down Green's tensors analogously to the treatment in Ref. [6],

$$\begin{aligned} \mathbf{G}_{\text{cav}}(x, z_1, z_2, \omega) = & \frac{i}{8\pi^2} \int_0^{\infty} dk_{\parallel} \frac{k_{\parallel}}{k_2^{\perp}} \int_0^{2\pi} d\phi_k e^{ik_{\parallel} x \cos \phi_k} \sum_{\sigma=s,p} \left(\frac{(r_{\sigma}^{21})^2 e^{ik_2^{\perp} (2d+z_1-z_2)}}{D_{\sigma}} \mathbf{e}_{\sigma+}^2 \otimes \mathbf{e}_{\sigma+}^2 + \mathbf{e}_{\sigma-}^2 \otimes \mathbf{e}_{\sigma+}^2 \right. \\ & \times \frac{r_{\sigma}^{21} e^{ik_2^{\perp} (2d-z_1-z_2)}}{D_{\sigma}} + \frac{r_{\sigma}^{21} e^{ik_2^{\perp} (z_2+z_1)}}{D_{\sigma}} \mathbf{e}_{\sigma+}^2 \otimes \mathbf{e}_{\sigma-}^2 + \left. \frac{(r_{\sigma}^{21})^2 e^{ik_2^{\perp} (2d-z_1+z_2)}}{D_{\sigma}} \mathbf{e}_{\sigma-}^2 \otimes \mathbf{e}_{\sigma-}^2 \right), \end{aligned} \quad (\text{S18})$$

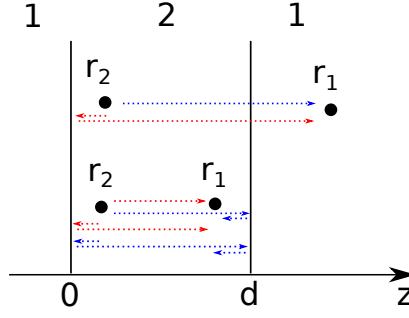


FIG. 1. Sketch of cavity geometry with photon paths connecting source and receiver points.

with reflection and transmission coefficients

$$r_s^{21} = \frac{k_2^\perp - k_1^\perp}{k_2^\perp + k_1^\perp}, \quad r_p^{21} = \frac{\epsilon_1 k_2^\perp - \epsilon_2 k_1^\perp}{\epsilon_1 k_2^\perp + \epsilon_2 k_1^\perp}, \quad (\text{S19})$$

$$t_s^{21} = \frac{2k_2^\perp}{k_2^\perp + k_1^\perp}, \quad t_p^{21} = \frac{k_1}{k_2} \frac{2\epsilon_2 k_2^\perp}{\epsilon_1 k_2^\perp + \epsilon_2 k_1^\perp}, \quad (\text{S20})$$

$$D_\sigma = 1 - (r_\sigma^{21})^2 e^{2ik_2^\perp d}. \quad (\text{S21})$$

For walls consisting of $n-1$ layers, one computes r_σ^{21} as above and infers the effective reflection coefficient of the stack layer by layer using the recursion relation

$$r_\sigma^{j+1,j} = \frac{\tilde{r}_\sigma^{j+1,j} + r_\sigma^{j,j-1} e^{2ik_j^\perp d_j}}{1 + \tilde{r}_\sigma^{j+1,j} r_\sigma^{j,j-1} e^{2ik_j^\perp d_j}}.$$

Here, $\tilde{r}_\sigma^{j+1,j}$ denotes two-layer coefficients analogously to Eq. (S19). The integral over ϕ_k in Eq. (S18) leads to cylindrical Bessel functions $J_n(x)$,

$$J_n(x) = \frac{1}{2\pi i^n} \int_0^{2\pi} d\phi e^{ix \cos \phi} \cos(n\phi). \quad (\text{S22})$$

The remaining integral over k^\parallel can be solved numerically by using an appropriate integration contour [7].

Furthermore, we encounter integrals of the form $\int dA' \mathbf{G}(\mathbf{r}, \mathbf{r}')$ that can be computed analytically. Integrating the Helmholtz Eq. (S12) and using the cylindrical symmetry, we obtain

$$\int dA' \mathbf{G}(\mathbf{r}, \mathbf{r}') = \text{diag}(\tilde{G}^\parallel(z, z'), \tilde{G}^\parallel(z, z'), 0), \quad (\text{S23})$$

$$[\partial_z^2 + k^2 \epsilon(z, \omega)] \tilde{G}^\parallel(z, z') = -\delta(z - z'). \quad (\text{S24})$$

This is also valid for the Green's tensor $\mathbf{G}_{\text{cav,out}}(\mathbf{r}, \mathbf{r}')$ that propagates light from a point inside of the cavity to a point outside of the cavity that is needed in the derivation of Eq. (5). The one-dimensional Helmholtz equation has the intuitive planar wave solutions (see Fig. 1)

$$\int dA' \mathbf{G}_{\text{cav,out}}(z, \mathbf{r}') = \text{diag}(1, 1, 0) \frac{it_{21} e^{ik(d-z') + ik_1(z-d)} + r_{21} e^{ik(d+z') + ik_1(z-d)}}{2k (1 - r_{21}^2 e^{2ikd})}, \quad (\text{S25})$$

$$\int dA' [\mathbf{G}_{\text{free}}(z, \mathbf{r}') + \mathbf{G}_{\text{cav}}(z, \mathbf{r}')] = \text{diag}(1, 1, 0) \frac{i e^{ik|z-z'|} + r_{21} e^{ik(z+z')} + r_{21} e^{ik(2d-z-z')} + r_{21}^2 e^{ik(2d-|z-z'|)}}{2k (1 - r_{21}^2 e^{2ikd})}. \quad (\text{S26})$$

Note that these results are not limited to the far field.

III. CONTINUOUS MEDIUM MODEL

In this section, we derive the transmission coefficient of the Fabry–Perot etalon, Eq. (6), from our microscopic interaction model. After averaging over the Maxwell-Boltzmann distribution, we retain only one polarizability $\bar{\alpha}_i =$

$\sqrt{\frac{a}{\pi}} \int_{-\infty}^{\infty} dv \alpha_i^{\pm} e^{-av^2}$ where $a = \frac{m}{2k_B T}$. As a result the coupled dipole model Eq. (3) can be rewritten into a single equation for the velocity averaged $\bar{\mathbf{d}}_i = \bar{\mathbf{d}}_i^+ + \bar{\mathbf{d}}_i^-$,

$$\bar{\mathbf{d}}_i = \bar{\alpha}_i \mathbf{E}_{\text{inc}} + \bar{\alpha}_i \sum_{j \neq i} \frac{k_0^2}{\epsilon_0} \mathbf{G}(\mathbf{r}_i, \mathbf{r}_j, \omega_0) \bar{\mathbf{d}}_j. \quad (\text{S27})$$

Averaging over the ground state populations, the polarizability tensor becomes diagonal $\bar{\alpha}(z) = \text{diag}[\alpha^{\parallel}(z), \alpha^{\parallel}(z), \alpha^{\perp}(z)]$. The transition from discrete atoms to a continuous gas is accomplished by the replacement $\sum_{j \neq i} \rightarrow N \int dV$. We introduce the susceptibility $\chi(z) = N\alpha^{\parallel}(z)/\epsilon_0$ and the normalized field $\tilde{E}_x(z) = d_x(z)/(\alpha^{\parallel}(z)E_0)$. The coupled dipole model Eq. (S27) becomes

$$\begin{aligned} \tilde{E}_x(z) &= \tilde{E}_{x,\text{inc}}(z) + k^2 \int_0^d dz' \int dA' G_{xx}(z, \mathbf{r}') \chi(z') \tilde{E}_x(z') \\ &\approx \tilde{E}_{x,\text{inc}}(z) + k^2 \chi \int_0^d dz' \int dA' G_{xx}(z, \mathbf{r}') \tilde{E}_x(z') \\ &= t_{12} \frac{e^{ikz} + r_{21} e^{ik(2d-z)}}{1 - r_{21}^2 e^{2ikd}} + \frac{ik\chi}{2} \int_0^d dz' \tilde{E}_x(z') \frac{e^{ik|z-z'|} + r_{21} e^{ik(z+z')} + r_{21} e^{ik(2d-z-z')} + r_{21}^2 e^{ik(2d-|z-z'|)}}{1 - r_{21}^2 e^{2ikd}}. \end{aligned} \quad (\text{S28})$$

In the second step, we neglected the non-collisional atom-wall interactions, replacing $\alpha^{\parallel}(z)$ with a constant α^{\parallel} . This approximation is valid in a regime where density-dependent interactions dominate as argued in the main text. In Eq. (S28), we do not explicitly account for the singular contribution of the free space Green's tensor (S13). Its effect can be incorporated by inserting the Lorentz-Lorenz shift into χ and redefining $\tilde{E}_x(z)$ as the locally corrected field. The solution of Eq. (S29) then assumes the intuitive form

$$\tilde{E}_x(z) = \frac{\tilde{t}_{12}(e^{ikn_G z} + \tilde{r}_{21} e^{ikn_G(2d-z)})}{1 - \tilde{r}_{21}^2 e^{2ikn_G d}}, \quad (\text{S30})$$

with new Fresnel coefficients $\tilde{t}_{12}, \tilde{r}_{21}$ between cavity walls and the refractive index $n_G = \sqrt{1 + N\alpha^{\parallel}/\epsilon_0}$ of the gas. Inserting this result into the continuous version of Eq. (5), we obtain the transmission profile of the Fabry-Perot etalon

$$t = \frac{t_{12} t_{21} e^{id(k-k_1)}}{1 - r_{21}^2 e^{2ikd}} + \frac{ik\chi}{2} e^{id(k-k_1)} \int_0^d dz \frac{e^{-ikz} + r_{21} e^{ikz}}{1 - r_{21}^2 e^{2ikd}} t_{21} \tilde{E}_x(z) = \frac{\tilde{t}_{12} \tilde{t}_{21} e^{id(kn_G - k_1)}}{1 - \tilde{r}_{21}^2 e^{2in_G kd}}. \quad (\text{S31})$$

IV. COLLECTIVE LAMB SHIFT

In this section, we derive the collective Lamb shift of a continuous atomic slab in free space. In the low density limit, one can approximate the solution of Eq. (S28) by considering only a single scattering event (first Born approximation). In free space, the result reads

$$\tilde{E}_x \approx \tilde{E}_x^{(0)} + \tilde{E}_x^{(1)} = e^{ikz} + k^2 \int_0^d dz' \int dA' G_{xx}(z, \mathbf{r}') \chi e^{ikz'}. \quad (\text{S32})$$

The transmission coefficient according to Eq. (S31) then assumes the form

$$t = 1 + \frac{ik\chi d}{2} (1 + \chi\xi), \quad \xi = \frac{k^2}{d} \int_0^d dz \int_0^d dz' \int dA' G_{xx}(z, \mathbf{r}') e^{ik(z'-z)}. \quad (\text{S33})$$

We can express the susceptibility $\chi = \frac{3\Delta_{\text{LL}}}{\delta + i/2\Gamma_0}$ in terms of the Lorentz-Lorentz shift $\Delta_{\text{LL}} = -\frac{N d_{eg}^2}{3\epsilon_0 \hbar (2J_g + 1)}$, where we assumed equally populated ground states with $\sum_{\mu, \nu} f_{i\mu}^{g} \mathbf{d}_{\mu\nu}^{ge} \otimes \mathbf{d}_{\nu\mu}^{eg} = \mathbf{I} \frac{d_{eg}^2}{(2J_g + 1)}$. Employing the Taylor expansion $\frac{1}{1-x} \approx 1 + x$ for $x \ll 1$, we can approximate the transmission profile by a Lorentz curve

$$t \approx 1 - \frac{kd\chi}{2i} \frac{1}{1 - \chi\xi} \quad (\text{S34})$$

$$= 1 - \frac{3\Delta_{\text{LL}} kd}{2i(\delta - 3\Delta_{\text{LL}} \text{Re} \xi) + 6\Delta_{\text{LL}} \text{Im} \xi - \Gamma_0}, \quad (\text{S35})$$

from which we can read off the collective Lamb shift. The resulting expression is identical to Eq. (4.1) in the original derivation of the collective Lamb shift by Friedberg *et al.* [8], which reads

$$\Delta = 3\Delta_{\text{LL}}\text{Re}\xi = \frac{3\Delta_{\text{LL}}k^2}{d}\text{Re}\int_0^d dz \int_0^d dz' \frac{i}{2k} e^{ik|z'-z|} e^{ik(z'-z)} \quad (\text{S36})$$

$$= -\frac{3\Delta_{\text{LL}}}{4} \left(1 - \frac{\sin(2kd)}{2kd}\right). \quad (\text{S37})$$

Subsequently, Friedberg *et al.* added a term Δ_{LL} accounting for the local-field correction that stems from the singularity of the free-space Green's tensor, Eq. (S13). We obtain the collective Lamb shift from an entirely classical theory.

V. FITTING FUNCTION

Here, we discuss the fitting function used to extract the parameters Δ_p, Γ_p . Both parameters modify the susceptibility of the vapor $\chi(z)$ for which we have to solve a continuous version of the coupled dipole model that accounts for non-collisional atom-wall interactions. Abbreviating $P_x(z) = \chi(z)\tilde{E}_x(z)$, Eq. (S28) becomes

$$\tilde{E}_{x,\text{inc}}(z) = \frac{1}{\chi(z, \Delta_p, \Gamma_p)} P_x(z) - k^2 \int_0^d dz' \int dA' G_{xx}(z, \mathbf{r}') P_x(z'). \quad (\text{S38})$$

The z' integral can be approximated by a Gauss–Laguerre quadrature, and the resulting linear set of equations is solved for $P_x(z)$. Eventually, one obtains the transmission profile

$$t = \frac{t_{12}t_{21}e^{id(k-k_1)}}{1 - r_{21}^2 e^{2ikd}} + \frac{ik}{2} e^{id(k-k_1)} \int_0^d dz \frac{e^{-ikz} + r_{21}e^{ikz}}{1 - r_{21}^2 e^{2ikd}} t_{21} P_x(z). \quad (\text{S39})$$

The susceptibility $\chi(z) = N\alpha^{\parallel}(z)/\epsilon_0$ is computed from the ground-state averaged polarizability

$$\alpha(z) = \frac{1}{(2J_g + 1)} \sum_{\mu,\nu} \alpha_{\mu\nu}^{ge}(z) = \text{diag}[\alpha^{\parallel}(z), \alpha^{\parallel}(z), \alpha^{\perp}(z)]. \quad (\text{S40})$$

It contains an average over the Maxwell–Boltzmann velocity distribution

$$\begin{aligned} \alpha_{\mu\nu}^{ge}(z) &= -\frac{1}{\hbar} \mathbf{d}_{\mu\nu}^{ge} \otimes \mathbf{d}_{\nu\mu}^{eg} \sqrt{\frac{a}{\pi}} \int_{-\infty}^{\infty} dv \frac{1}{B_{\mu\nu} \mp kv} e^{-av^2} \\ &= -\frac{1}{\hbar} \mathbf{d}_{\mu\nu}^{ge} \otimes \mathbf{d}_{\nu\mu}^{eg} \frac{\sqrt{\pi a}}{k} \left(D \left(\frac{\sqrt{a} B_{\mu\nu}}{k} \right) - i e^{-\frac{a B_{\mu\nu}^2}{k^2}} \text{sign} \left(\frac{\text{Im} B_{\mu\nu}}{k} \right) \right), \end{aligned} \quad (\text{S41})$$

where $D(x) = e^{x^2} \int_0^x dt e^{-t^2}$ is the Dawson function, $a = \frac{m}{2k_B T}$ and

$$B_{\mu\nu} = \delta - \left[\omega_{\text{CP}}^{ge}(z) + \Delta_p \right] + \frac{i}{2} \left[\Gamma_{\nu}^e(z) + \Gamma_p \right]. \quad (\text{S42})$$

-
- [1] Ho Trung Dung, Ludwig Knöll, and Dirk-Gunnar Welsch, “Resonant dipole-dipole interaction in the presence of dispersing and absorbing surroundings,” *Physical Review A* **66**, 063810 (2002).
 - [2] Stefan Yoshi Buhmann, Ludwig Knöll, Dirk-Gunnar Welsch, and Ho Trung Dung, “Casimir-polder forces: A nonperturbative approach,” *Physical Review A* **70**, 052117 (2004).
 - [3] Mark D Lee, Stewart D Jenkins, and Janne Ruostekoski, “Stochastic methods for light propagation and recurrent scattering in saturated and nonsaturated atomic ensembles,” *Physical Review A* **93**, 063803 (2016).
 - [4] Stefan Yoshi Buhmann, *Dispersion Forces II: Many-Body Effects, Excited Atoms, Finite Temperature and Quantum Friction*, Vol. 248 (Springer, 2013).
 - [5] T Peyrot, Y R P Sortais, J-J Greffet, A Browaeys, A Sargsyan, J Keaveney, I G Hughes, and C S Adams, “Optical transmission of an atomic vapor in the mesoscopic regime,” *Phys. Rev. Lett.* **122**, 113401 (2019).

- [6] Stefan Yoshi Buhmann, *Dispersion forces I: Macroscopic quantum electrodynamics and ground-state Casimir, Casimir-Polder and van der Waals Forces*, Vol. 247 (Springer, 2013).
- [7] Michael Paulus, Phillipe Gay-Balmaz, and Olivier J F Martin, “Accurate and efficient computation of the greens tensor for stratified media,” *Phys. Rev. E* **62**, 5797 (2000).
- [8] Richard Friedberg, Sven Richard Hartmann, and Jamal T Manassah, “Frequency shifts in emission and absorption by resonant systems of two-level atoms,” *Phys. Rep.* **7**, 101–179 (1973).